Cobalt nanorods fully encapsulated in carbon nanotube and magnetization measurements by off-axis electron holography

Takeshi Fujita[a)]
International Frontier Center for Advanced Materials, Institute for Materials Research, Tohoku University, Aoba-ku, Sendai, Miyagi 980-8577, Japan

Yasuhiko Hayashi
Department of Environmental Technology and Urban Planning, Nagoya Institute of Technology, Gokiso, Showa, Nagoya 466-8555, Japan

Tomoharu Tokunaga
Department of Materials Science and Engineering, Faculty of Engineering, Kyushu University, Fukuoka 812-8581, Japan

Kazuo Yamamoto
Japan Society for the Promotion of Science, Center for Solid State Science, Arizona State University, Tempe, Arizona 85287-1704

(Received 3 February 2006; accepted 2 May 2006; published online 15 June 2006)

Fully encapsulated face-centered-cubic (fcc) Co nanorods in multiwalled carbon nanotubes were produced by microwave plasma enhanced chemical vapor deposition. Quantitative magnetization measurements of the Co nanorods were carried out by off-axis electron holography using a theoretical cylindrical model. The component of magnetic induction was then measured to be 1.2 ± 0.1 T, which is lower than the expected saturation magnetization of fcc Co of 1.7 T. The reason for the reduced magnetic component was discussed. © *2006 American Institute of Physics*.
[DOI: 10.1063/1.2213202]

The encapsulation of ferromagnetic metals in carbon nanotubes (CNTs) is attractive for spin electronics because of their high potential for application in highly dense recording media. Encapsulation of Ni, Co, Fe,[1] and FeCo (Ref. 2) in CNTs has been reported and characterized by transmission electron microscopy (TEM), and the magnetic properties such as coercivity and saturation magnetization have been extensively measured. In our recent study, we fully encapsulated Pd nanometer particles in multiwalled CNTs (MWCNTs) on a Mo TEM grid by microwave plasma enhanced chemical vapor deposition (MPECVD).[3] The MPECVD technique has also realized the production of fully encapsulated Co in MWCNTs showing a possibly significant magnetization from an isolated nanorod. Electron holography is a technique that provides the relative phase shift of the electron wave after passing through the sample.[4] This phase shift is sensitive to the electrostatic potential and the component of magnetic induction in the plane of the specimen, and it can be quantitatively evaluated at high spatial resolutions close to the nanometer scale. In this study, we utilize off-axis electron holography to observe the remanent states of the fully encapsulated Co nanometer particle at room temperature.

A primary Co metal layer (15 nm in thickness) was deposited on a Si substrate by a vacuum evaporation method. The Si substrate was then transferred into the MPECVD system. The vacuum inside the chamber was below 10^{-8} Torr. The substrate was then heated up to 973 K and maintained for 600 s in a H_2 gas atmosphere of 50 Torr. Then, the vertically aligned CNTs (VA-CNTs) were grown while the feed gas (CH_4) was introduced at a pressure of 20 Torr with a negative bias of 400 V applied to the substrate for 600 s. In order to obtain an effective substrate bias, the substrate was located on a quartz board. The heating of the substrate was stopped, and it was cooled down in a H_2 gas atmosphere of 50 Torr. The Co filled VA-CNTs on the substrate were then observed by using a scanning electron microscope (SEM) for verification. TEM samples of about 1 mm thickness were carved from the Si substrate and attached to a commercial Mo TEM grid. For holographic experiments, a Philips CM200 TEM with a Schottky thermal field emission gun, an electrostatic biprism, and a 1024×1024 pixel Gatan 794 multiscan charge-coupled device (CCD) camera was used at 200 keV. An electrostatic potential of 130 V was applied to the biprism wire for recording a hologram. The phase shift detected by electron holography can be expressed as the sum of an inner potential φ_{MIP} and the magnetic component φ_{MAG} as follows:[5]

$$\Delta\varphi(x,y) = \varphi_{\mathrm{MIP}} + \varphi_{\mathrm{MAG}} = C_E \int V_0(x,z)dz - \frac{e}{\hbar}\int\int B_{\perp}(x,z)dxdz, \quad (1)$$

where x is a direction in the plane of the sample, z is the electron beam direction, C_E is a wavelength-dependent constant taking a value of 7.29×10^6 rad V^{-1} M^{-1} at an accelerating voltage of 200 kV, V_0 is the mean inner potential, e is the elementary charge, $\hbar = h/2\pi$ where h is Planck's constant, and $B_{\perp}$ is the in-plane component of magnetic induction perpendicular to x and z. A Lorentz minilens below the lower objective pole piece was used for magnetic imaging such that the sample was located in an almost magnetic-field-free environment when the normal objective lens was switched off.[6] The two factors—φ_{MIP} and φ_{MAG}—can be

[a)]Author to whom correspondence should be addressed; electronic mail: tfujita@imr.tohoku.ac.jp

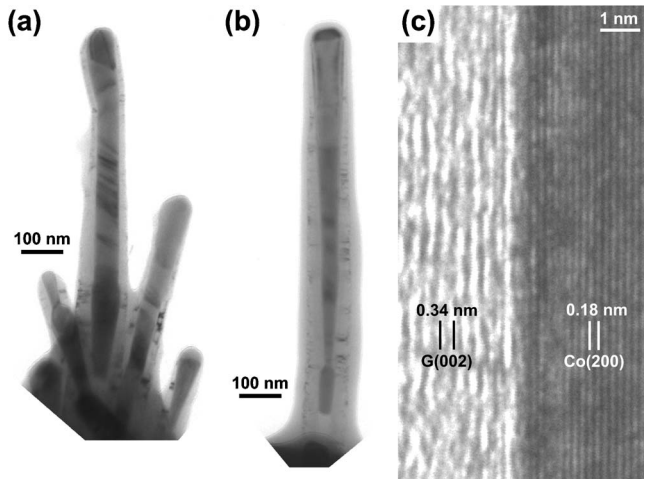

FIG. 1. Representative bright-field TEM and HRTEM images; (a) bundle of MWCNTs fully encapsulating Co nanorods; (b) MWCNT encapsulating a cone shaped Co nanorod; (c) typical HRTEM image taken at the interface between graphite and fcc Co. The graphite (002) plane is parallel to the fcc Co (200) plane.

separately measured by using *in situ* magnetization reversal.[7] Two pairs of holograms were recorded at the same position; the sample was tilted once by ±30° and the normal object lens was fully excited with a magnetic field of 1 T. The field was then turned off, and the sample was tilted back to 0°. Finally, a hologram recording was conducted. Each retrieved phase image from the two recorded holograms yields a different image of φ_{MAG} according to Eq. (1).

Figures 1(a) and 1(b) are the typical bright-field TEM images of Co filled VA-CNTs. Figure 1(a) shows the case in which the diameter of encapsulated Co in the MWCNT at the center is almost the same along the growth direction. Figure 1(b) shows the case in which Co is cone shaped and the diameter is reduced from the top to the bottom. Co deposited on the substrate functions as a catalyst to produce MWCNTs, and it is encapsulated during the growth of MWCNTs; therefore, when the amount of Co on the substrate becomes insufficient during the MPECVD process, the diameter of the resulting encapsulated Co nanorod becomes smaller than that at the top region. The face-centered-cubic (fcc) structure of Co was confirmed by a selected area diffraction pattern (SADP).

Figure 1(c) shows a high-resolution transmission electron microscopy (HRTEM) image of the interface between graphite (G) and fcc Co. The lattice constant of fcc Co is 0.3545 nm,[8] and we observed a clear match confirming that the Co (200) plane is usually parallel to G (002). However, it is noteworthy that the fcc Co nanorods inside MWCNTs were often polycrystalline. We believe that the polycrystalline structure is promoted because of the poor crystallinity of the graphite, as observed in Fig. 1(c), and the large inner diameter of MWCNTs exceeding 50 nm. Tyagi *et al.* reported that the strict relationship between encapsulated Co and the nanotube was valid for the tubes with an inner diameter of up to 20 nm.[9] In addition, no particular orientation relationships between the Co grains were found by using the convergent beam electron diffraction technique, but further investigation on the polycrystalline structure is necessary. In this study, we focus on the remanent state of the Co nanorod.

Figure 2(a) shows a hologram taken from the Co nanorod shown in Fig. 1(a). Figure 2(b) shows the color contour map of φ_{MAG} retrieved from the two holograms mentioned above. The magnetic induction passes through the entire inner Co nanorod and emerges from the top. Figure 2(c) shows a hologram of the Co nanorod shown in Fig. 1(b), and the corresponding φ_{MAG} is shown in Fig. 2(d). It is noteworthy that the magnetic flux converges only near the top region; the reason for this is discussed later.

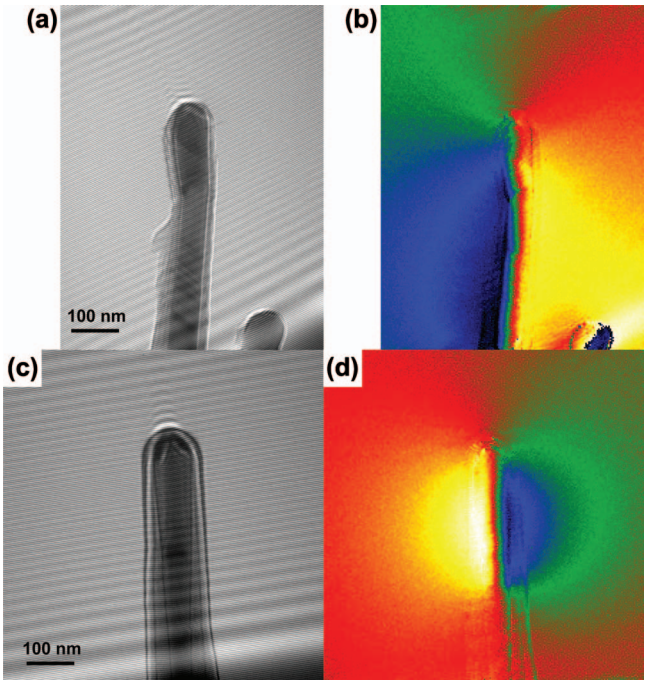

FIG. 2. (Color) (a) Hologram taken from the MWCNT in Fig. 1(a); (b) shows the color contour map of the corresponding magnetic component φ_{MAG} of the reconstructed phase; (c) hologram taken from the MWCNT in Fig. 1(b); (d) shows the color contour map of the corresponding φ_{MAG}. The magnetic flux emerging from the nanorod is limited only near the top region of the Co rod.

For the quantitative phase analysis of the magnetic flux on a magnetic nanorod, the theoretical calculation that takes the fringing magnetic field into account is essential. The Co nanorod shape can be approximated by a cylindrical rod with uniform magnetization and radius R and length $2L$ at the origin on an x-y orthogonal coordinate system. The cylindrical direction is parallel to the y axis. According to Beleggia and Zhu,[10] the phase shift φ_{MAG} for an elongated cylindrical magnet can be obtained in Fourier space. We derived

$$\varphi_{\mathrm{MAG}}(\mathbf{k}) = \frac{4\pi^2 i B_\perp RL}{\phi_0} \frac{k_y \cos\beta - k_x \sin\beta}{k_x k_\perp^2} \times J_1(k_x R)\,\mathrm{sinc}(k_y L), \tag{2}$$

where $\mathbf{k}=(k_x,k_y)$ is the vector in Fourier space $k_\perp = (k_x^2+k_y^2)^{1/2}$, $B_\perp$ the magnetic induction, R the radius, L the half length of the cylindrical particle, $\phi_0=h/2e$, β the angle between magnetic direction $\mathbf{M}$ and the x axis, $J_1(x)$ the Bessel function of the first order, and $\mathrm{sinc}(x)\equiv(\sin x)/x$. The phase shift in real space can be calculated by the inverse Fourier transform of Eq. (2). We evaluated Eq. (2) for $B_\perp$ with parameters of $B_\perp=1.2$ T, $R=32$ nm, $L=150$ nm, and $\beta=90°$ and compared it with the experimental phase profile of φ_{MAG} across the center region from A to B in Fig. 3(a) and the theoretical profile across the center region of the computed object. Figure 3(b) shows both the profiles of the plotted experimental and calculated phase values. The good

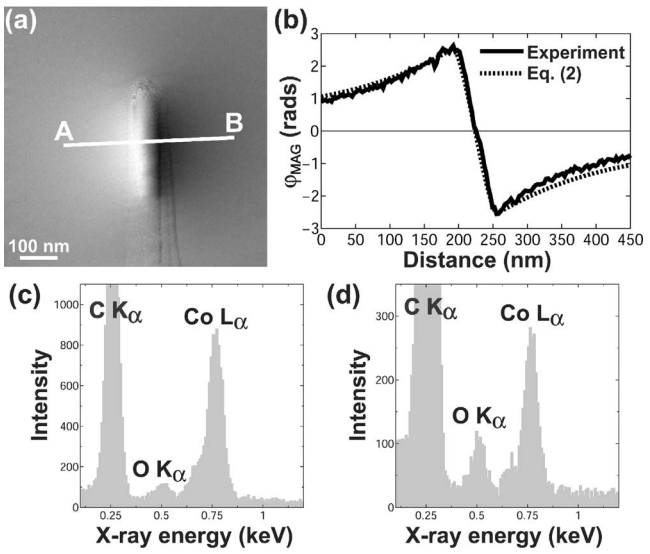

FIG. 3. (a) φ_{MAG} of the cone shaped Co nanorod of Fig. 1(b); (b) phase profile across the nanorod from A to B in (a); (c) x-ray profile acquired from the magnetized top region; (d) x-ray profile acquired from the nonmagnetized bottom region.

agreement of both the profiles implies that the theoretical model of Eq. (2) is valid for the quantitative analysis of $B_\perp$ for cylindrical magnetic materials by electron holography. We examined other Co nanorods, shown in Fig. 1(b), to precisely measure the value of $B_\perp$. The measured values of $B_\perp$ did not vary with size and were found to be within 1.2 ± 0.1 T, which is lower than the value 1.7 T of fcc Co.[11] Some reasons for the decrease in $B_\perp$ must be considered. The rapid quenching of Co from high temperature to room temperature during the MPECVD process may cause a disorder state in the Co and result in a decrease from 1.7 T to 1.2 T.[12] In addition, the magnetization process of fcc Co is easy in the $\langle 111\rangle$ direction and difficult in the $\langle 100\rangle$ direction.[13] The HRTEM result shows that fcc Co (200) planes tend to be parallel to G (002) planes; therefore, the direction in which the magnetization process is easy is not parallel to the actual magnetization direction. Furthermore, we found that another possible reason for this is the surface oxidation of Co nanorods. Figures 3(c) and 3(d) show the result of x-ray microanalysis using a 5 nm electron probe placed at the top and bottom regions of the Co nanorod shown in Fig. 1(b), respectively. Evidently, O $K\alpha$ was detected; therefore, the remanent magnetization may have been degraded by the oxidation for the formation of CoO.

According to Hill *et al.*,[14] the possible partial oxidation of Co nanorods leads to an isotropic superparamagnetic behavior with a decrease in the size of the rod. With regard to the cone shaped Co nanorod shown in Fig. 1(b), the partial oxidation intensifies with a decrease in the diameter. The ratio of the integrated intensity O $K\alpha$/Co $L\alpha$ is 0.40 for the bottom region and 0.11 for the top region, but the integrated O $K\alpha$ itself is almost the same, 584 counts for Fig. 3(c) and 687 counts for Fig. 3(d). Therefore, the surface of the Co nanorod is uniformly oxidized from the top to the bottom such that the decrease in the diameter shrinks the magnetized core region, and the magnetic signal is not detectable because of the superparamagnetism. It should be noted that we verified the uniform Co oxidation by another x-ray analysis that took into account the O $K\alpha$ intensity from only the MWCNT.

In conclusion, we have obtained MWCNTs fully encapsulating Co nanorods on a Si substrate using MPECVD process. Quantitative magnetization measurements of cylindrical magnets were experimentally established by electron holography. The measured values of $B_\perp$ were determined to be within 1.2 ± 0.1 T, which is lower than the value 1.7 T of fcc Co. The partial oxidation of the ferromagnetic nanorod during the process and the magnetization direction, in which the magnetization process is not easy, may play an important role in the determination of the quality of the remanent states.

This study was supported by the Japan Society for the Promotion of Science for the award of Postdoctoral Fellowships for Research Abroad. The authors acknowledge the John M. Cowley Center for High Resolution Electron Microscopy for providing the use of facilities. One of the authors (Y.H.) would like to thank Professor Gehan Amaratunga at the University of Cambridge and Professor Ravi Silva at the University of Surrey for their useful discussions. This work was also partly supported by a Grant-in Aid for Scientific Research (Houga-16651065) of the Ministry of Education, Culture, Sports, Science and Technology (MEXT), Japan.

[1] A. Leonhardt, M. Ritschel, R. Kozhuharova, A. Graff, T. Mühl, R. Huhle, I. Mönch, D. Elefact, and C. M. Schneider, Diamond Relat. Mater. **12**, 790 (2003).
[2] A. L. Elías, J. A. Rodriguez-Manzo, M. R. McCartney, D. Golberg, A. Zamudio, S. E. Baltazar, F. López-Urías, E. Muñoz-Sandoval, L. Gu, C. C. Tang, D. J. Smith, Y. Bando, H. Terrones, and M. Terrones, Nano Lett. **5**, 467 (2005).
[3] S. Toh, K. Kaneko, Y. Hayashi, T. Tokunaga, and W.-J. Moon, J. Electron Microsc. **53**, 149 (2004).
[4] W. J. de Ruijter and J. K. Weiss, Ultramicroscopy **50**, 269 (1993).
[5] L. Reimer, *Transmission Electron Microscopy* (Springer, Berlin, 1989).
[6] M. R. McCartney, D. J. Smith, R. F. C. Farrow, and R. F. Mark, J. Appl. Phys. **82**, 2461 (1997).
[7] R. E. Dunin-Borkowski, M. R. McCartney, D. J. Smith, and S. S. P. Parkin, Ultramicroscopy **74**, 61 (1998).
[8] S. Ram, Mater. Sci. Eng., A **304–306**, 923 (2001).
[9] P. K. Tyagi, A. Misra, M. K. Singh, D. S. Misra, J. Ghatak, P. V. Satyam, and F. Le Normand, Appl. Phys. Lett. **86**, 253110 (2005).
[10] M. Beleggia and Y. Zhu, Philos. Mag. **83**, 1045 (2003).
[11] M. J. Besnus, A. J. P. Meyer, and R. Berninge, Phys. Lett. **32A** 192 (1970).
[12] H. P. Meyers and W. Sucksmith, Proc. R. Soc. London, Ser. A **207**, 427 (1951).
[13] T. Suzuki, D. Weller, C.-A. Chang, R. Savoy, T. Huang, B. A. Gurney, and V. Speriosu, Appl. Phys. Lett. **64**, 2736 (1994).
[14] T. Hill, M. Mozaffari-Afshar, J. Schmidt, T. Risse, and H.-J. Freund, Surf. Sci. **429**, 246 (1999).